The structure of the paraelectric and incommensurate phases of $TlGaSe_2$

1990 J. Phys.: Condens. Matter 2 3699

(http://iopscience.iop.org/0953-8984/2/16/001)

J. Phys.: Condens. Matter 2 (1990) 3699–3712. Printed in the UK

The structure of the paraelectric and incommensurate phases of $TlGaSe_2$

D F McMorrow†, R A Cowley‡, P D Hatton† and J Banys†‡§

† Department of Physics, University of Edinburgh, Mayfield Road, Edinburgh EH9 3JZ, UK

‡ Clarendon Laboratory, Parks Road, Oxford OX1 3PU, UK

Received 1 December 1989, in final form 23 February 1990

Abstract. The structure of $TlGaSe_2$ has been studied by triple-crystal x-ray scattering techniques. At room temperature in the paraelectric phase the structure is believed to be $C2/c$, but we found that some of the (h, h, l) Bragg reflections, those with h odd, are broadened along the c^* direction. This is shown to arise because of faults in the stacking of the atomic sheets perpendicular to c^*. A simple model is developed for the scattering which suggests that on average a stacking fault occurs in the single crystal about once every four planes. Between 117 and 110 K the crystal has an incommensurate structure with a wavevector $(\delta, \delta, \frac{1}{4})$ where $\delta \simeq 0.02$ reciprocal lattice units. At 110 K, δ jumps discontinuously to zero to produce a commensurate phase. These results confirm the earlier suggestions of an incommensurate phase in $TlGaSe_2$.

1. Introduction

$TlGaSe_2$ is a member of the ternary semiconducting chalcogenides with the chemical formula ABX_2 (A and B being metal atoms while X is a chalcogenide). This family is of interest because they are semiconducting (Guseinov *et al* 1967), have large temperature dependent dielectric constants (Aliev *et al* 1984), undergo structural phase transitions (Abdullaev *et al* 1977), and are photoconducting (Offergeld 1963). The most studied members of the family are $TlGaSe_2$ and $TlInS_2$. At room temperature both materials are reported (Henkel *et al* 1982) to have a monoclinic structure, $C2/c$, and on cooling there are two transitions at T_i and T_c. In the case of $TlInS_2$, the phase between $T_i = 216$ K and $T_c = 200$ K has been shown by neutron diffraction to be a modulated phase (Vakhrushev *et al* 1984b), with a wavevector $\boldsymbol{q}_i = (\delta, \delta, \frac{1}{4})$ where $\delta \simeq 0.02$, while below T_c there is a lock-in transition to a distorted structure with $\boldsymbol{q}_c = (0, 0, \frac{1}{4})$. In the case of $TlGaSe_2$ the existence of an incommensurate phase between $T_i = 120$ K and $T_c = 107$ K was inferred from dielectric spectroscopy (Volkov *et al* 1983, Banys *et al* 1987) and Raman scattering (see, for example, Durnev *et al* 1989). A neutron diffraction study of $TlGaSe_2$ by Vakhrushev *et al* (1984a) did not find any evidence for an incommensurate

§ Permanent address: Faculty of Physics, Vilnius University, 232054 Vilnius, Lithuania, USSR.

0953-8984/90/163699 + 14 $03.50

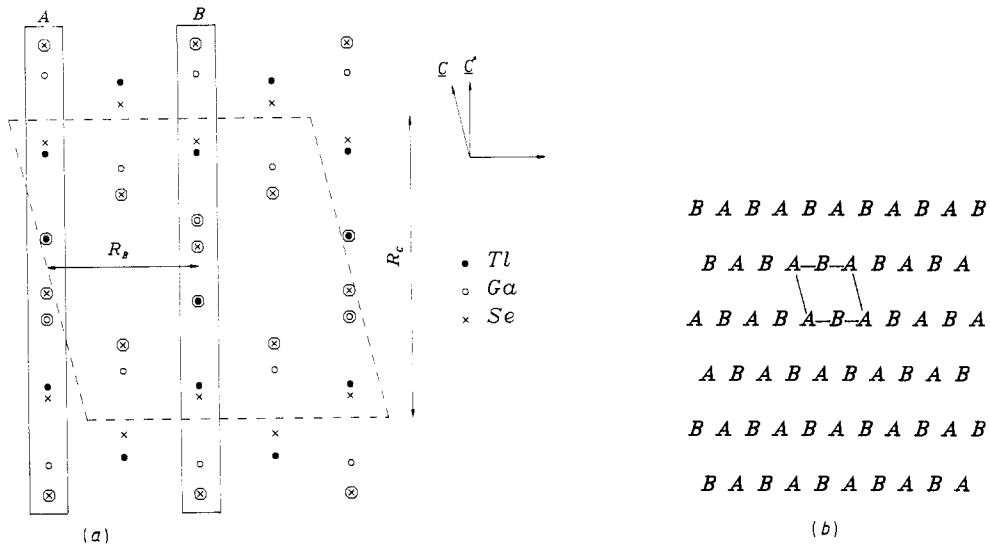

Figure 1. A projection of the structure of $TlGaSe_2$ on the $(1\bar{1}0)$ plane. The monoclinic unit cell is shown by the parallelogram and the two repeating units by boxes labelled *A* and *B* in (*a*). The symbols surrounded by circles indicate where there are two coincident atoms in the projection. The stacking of the *A* and *B* units in this plane is illustrated in (*b*).

structure, but below T_c the results showed there was a quadrupoling of the unit cell along the *c* axis.

The present x-ray scattering study of $TlGaSe_2$ was undertaken to clarify the nature of the incommensurate phase. The scattering was first studied at room temperature, and it was found that the Bragg reflections (h, h, l) with h even, were well defined, but that the scattering occurring near the (h, h, l) reflections with h odd was not well defined, but elongated along the c^* axis. This result led us to conduct a detailed study of the high-temperature phase, and the experimental results are reported in section 3.1, and are subsequently discussed in terms of a simple model in section 3.2. (The experimental arrangement is described in section 2.) In section 4 we present evidence for the existence of an incommensurate phase between T_i and T_c and describe the temperature dependence of the scattering. Measurements of the scattering below T_c are described in section 5.

2. Experimental considerations

2.1. The x-ray diffractometer

The measurements were performed using a triple-crystal x-ray diffractometer situated on a GEC Avionics GX21 rotating-anode generator operating at 3 kW. Experiments were initially performed using flat pyrolytic graphite crystals to monochromate the Cu $K\alpha_1$ radiation and to analyse the scattering from the sample crystal. The resolution in the scattering plane is then about 0.02 $Å^{-1}$. Some experiments were later performed with identical germanium crystals as monochromator and analyser using the (111) planes to give an in-plane resolution of about 5×10^{-4} $Å^{-1}$. The resolution perpendicular to

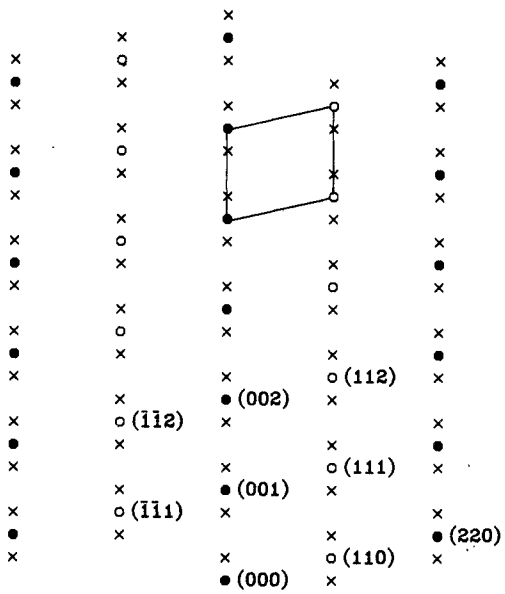

Figure 2. The reciprocal lattice of $TlGaSe_2$. The Brillouin zone is shown by the parallelogram and the well-defined reflections (h, h, l) with h even are solid points. The reflections with h odd are extended along $[0, 0, l]$ and are shown by open circles. The extra reflections occurring in the ferroelectric low-temperature phase are shown by crosses.

the scattering plane was defined by slits and was about 0.05 $Å^{-1}$. Detailed accounts of the resolution function of a triple-crystal diffractometer are given by Cowley (1987) and by Lucas *et al* (1989).

2.2. *The sample*

The single crystal of $TlGaSe_2$ was grown by the Bridgman method, and had previously been examined using dielectric techniques (Banys *et al* 1987). The sample was a semi-circular thin plane with a radius of 4.5 mm, and with the face parallel to the ***a–b*** plane. The sample was mounted in a strain-free manner on the cold finger of a closed-cycle refrigerator which had a temperature stability of 0.05 K.

At room temperature the structure of $TlGaSe_2$ is reported to be $C2/c$ with a = 10.772 Å, b = 10.771 Å, c = 15.636 Å and β = 100.06° (Müller and Hahn 1978, Henkel *et al* 1982). The crystal was aligned with the [110] and [001] axes in the scattering plane. The structure as given by Henkel *et al* (1982) projected onto this plane is shown in figure 1, while the reciprocal lattice of the monoclinic structure is illustrated in figure 2. In this plane the structure consists of lines of atoms running perpendicular to the ⟨110⟩ axis and separated by 1.904 Å, as shown in figure 1(a). The structure can be described as having two sheets of atoms centred on each unit cell. The sequence of atoms in the sheet labelled B in figure 1(a) is opposite to that of the sheet labelled A. The displacement of the two units from one unit cell to the next is illustrated in figure 1(b), and because $\cos\beta$ = −0.254, or very close $-\frac{1}{4}$, the sheets in the next unit cell, one unit up the c axis, are positioned almost exactly mid-way between the units of the lower unit cell, figure 1(b). Consequently if the difference in the orientation of the two sheets was neglected, i.e. $A = B$, the two-dimensional structure of figure 1(b) would be centred tetragonal with a = 3.81 Å and c = 30.79 Å. The reciprocal lattice of such a structure would have the centred lattice shown in figure 2 by the filled points with h even.

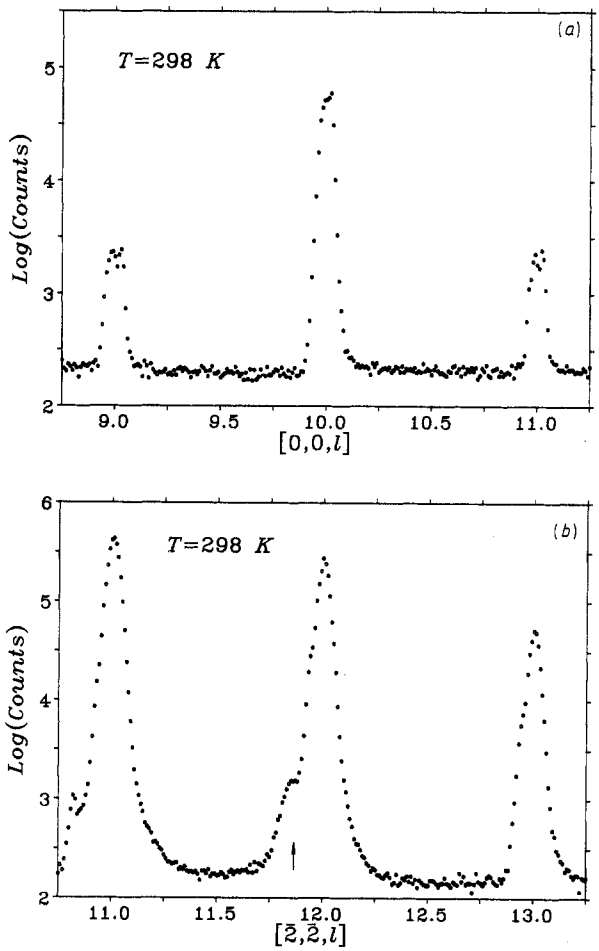

Figure 3. The x-ray scattering observed in the paraelectric phase at 298 K for a scan along $[0, 0, l]$ (a) and $[\bar{2}, \bar{2}, l]$ (b) using the low-resolution configuration. The vertical arrow indicates the calculated position of a powder line from the Cu block on which the sample was mounted.

3. The paraelectric structure

3.1. Experimental results

During initial measurements on the crystal, we discovered that some of the Bragg reflections were much broader along c^* than the instrumental resolution. Consequently a detailed study was made of the scattering using the low-resolution, pyrolytic graphite arrangement. It was found that the Bragg reflections of the type (h, h, l) with h even are well defined as shown by the scans along $[0, 0, l]$ and $[\bar{2}, \bar{2}, l]$ in figure 3. These figures show well-defined Bragg reflections, and little other scattering except for powder lines from the sample mounting block (indicated in these and all subsequent figures by vertical arrows). The reflections for $[0, 0, l]$ with l odd are observed to be weak; for the $C2/c$ space group they are systematically absent. This weak scattering probably arises from

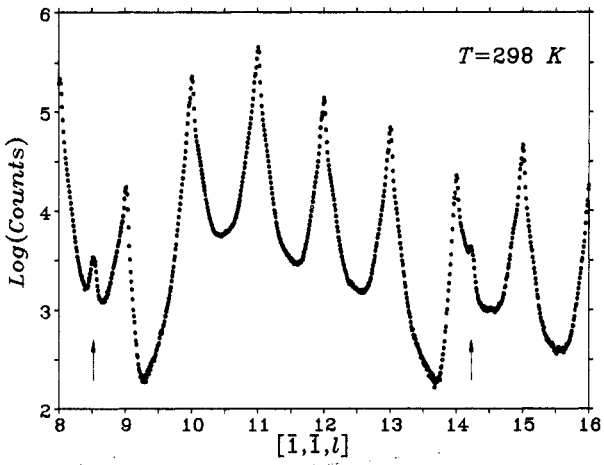

Figure 4. The x-ray scattering observed in the paraelectric phase at 298 K for a scan along $[\bar{1}, \bar{1}, l]$ using the low-resolution configuration. The minima in the scattering for $l = 9.3$ and $l = 13.7$ are due to zeros in the structure factor at these positions, and are discussed in the text.

multiple Bragg reflection, which may be significant due to the relatively low resolution used in these scans.

The scattering profiles of the (h, h, l) reflection with $h = \bar{1}$ is very different, as shown in figure 4. Each Bragg reflection along $[\bar{1}, \bar{1}, l]$ is considerably broader than the instrumental resoltuion, with wings extending to the zone boundary. The detailed form of the scattering varies from zone to zone. Scattering profiles similar to those observed along $[1, 1, l]$ were also obtained for the $[\bar{1}, \bar{1}, l]$ lines and $[3, 3, l]$ directions, as shown in figures 5 and 6. Normal to the c^* direction, all Bragg reflections were found to be approximately resolution limited.

In order to examine this behaviour in more detail, the scattering was also studied with the high-resolution, germanium arrangement. The results for the scattering near the (2, 2, 12) and (1, 1, 10) Bragg reflections are shown respectively in figures 7 and 8. The results for the (2, 2, 12) reflection show a peak which is resolution limited in the direction both parallel and perpendicular to c^*. In contrast, the results for the (1, 1, 10) peak show a resolution limited peak perpendicular to c^*, but along c^* a broad, diffuse component in addition to a sharp component. In the lower resolution experiments, figures 4–6, these two components could not be readily distinguished. The origin of this sharp component is not known. The diffuse peak is aligned exactly along c^*, with a full width at half maximum of $0.20(2)c^*$; perpendicular to c^* it is resolution limited.

3.2. A model of the structure

The nominal structure of $TlGaSe_2$ projected onto the (h, h, l) plane is shown in figure 1(a), and consists of lines of atoms whose positions are very closely parallel to c^*. There are two arrangements of the atoms within each unit cell, labelled A and B in figure 1(a). The way these units are arranged to form the complete structure is illustrated in figure 1(b). The two different units are simply related to one another through an inversion with respect to c^*.

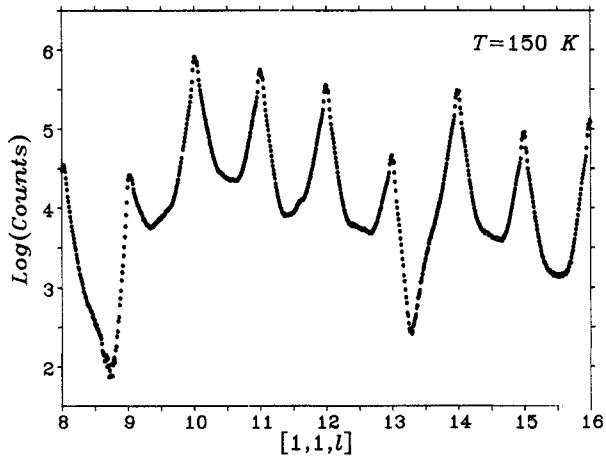

Figure 5. The x-ray scattering observed at 150 K in the paraelectric phase for scans along $[1, 1, l]$ using the low-resolution configuration. The minima in the scattering profile at $l = 8.7$ and $l = 13.3$ are due to zero values of the structure factor at these positions and are discussed in the text.

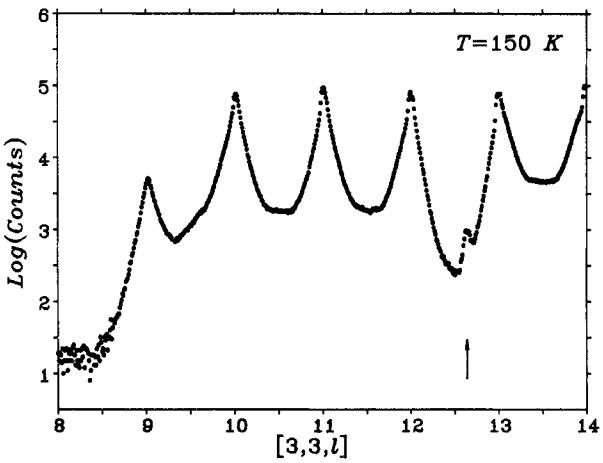

Figure 6. The x-ray scattering observed in the paraelectric phase at 150 K for a scan along $[3, 3, l]$ using the low-resolution configuration. The minimum in the scattering at $l = 12.3$ arises from the structure factor going to zero at this position. The region of reciprocal space for $l < 8.5$ corresponds to one of the forbidden zones in the extended face scattering geometry used in these experiments. These zones arise when either the incident or diffracted x-ray beam is obscured by the crystal face.

The structure factor of these units is given for a wavevector transfer, $\boldsymbol{Q}$, by

$$f(A, \boldsymbol{Q}) = \sum_{\kappa} f_{\kappa}(\boldsymbol{Q}) \exp(-W_{\kappa}) \exp(\mathrm{i}\,\boldsymbol{Q} \cdot \boldsymbol{R}(\kappa))$$

where κ is the index of the atom, $f_{\kappa}(\boldsymbol{Q})$ the x-ray atomic form factor, W_{κ} the Debye–Waller factor and $\boldsymbol{R}(\kappa)$ the position of each atom with respect to the centre of the unit.

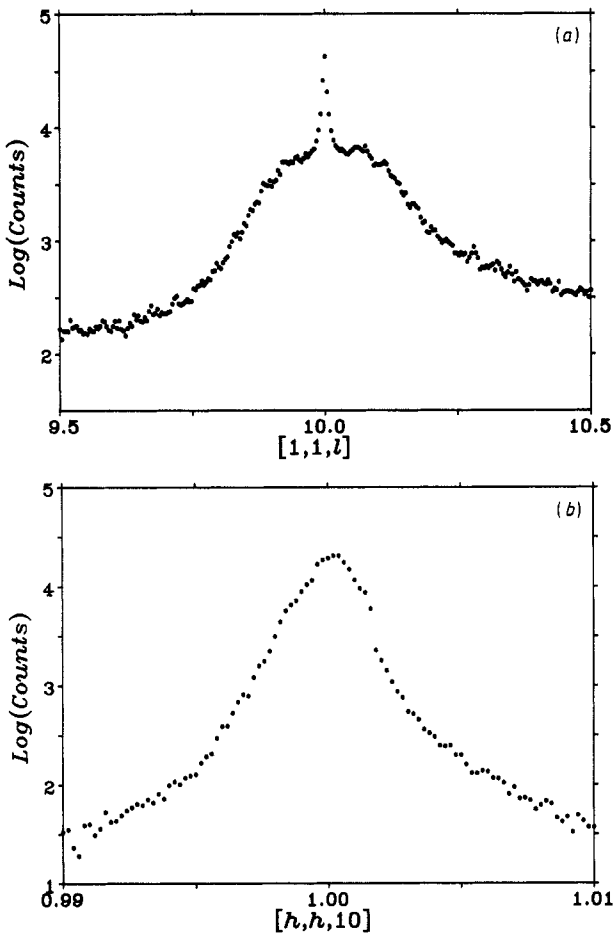

Figure 7. The x-ray scattering profiles of the (2, 2, 12) Bragg reflection measured in the paraelectric phase at 298 K for scans performed parallel (*a*) and perpendicular to c^* (*b*). The high-resolution configuration was used for these measurements. Note: we have plotted the lower figure with an expanded $\boldsymbol{Q}$ scale.

Since unit B consists of the same atoms but with $\boldsymbol{R}(\kappa)$ given by $-\boldsymbol{R}(\kappa)$, with respect to the centre of the unit,

$$f(B, \boldsymbol{Q}) = f(A, -\boldsymbol{Q})$$

provided that $f_\kappa(\boldsymbol{Q})$ is real and the Debye–Waller factor is approximated by the quadratic term in $\boldsymbol{Q}$. If the form factor is written as

$$f(A, \boldsymbol{Q}) = f_1(\boldsymbol{Q}) + \mathrm{i} f_2(\boldsymbol{Q})$$

then

$$f(B, \boldsymbol{Q}) = f_1(\boldsymbol{Q}) - \mathrm{i} f_2(\boldsymbol{Q})$$

and the structure factor of the scattering is given, by summing over the two units, as

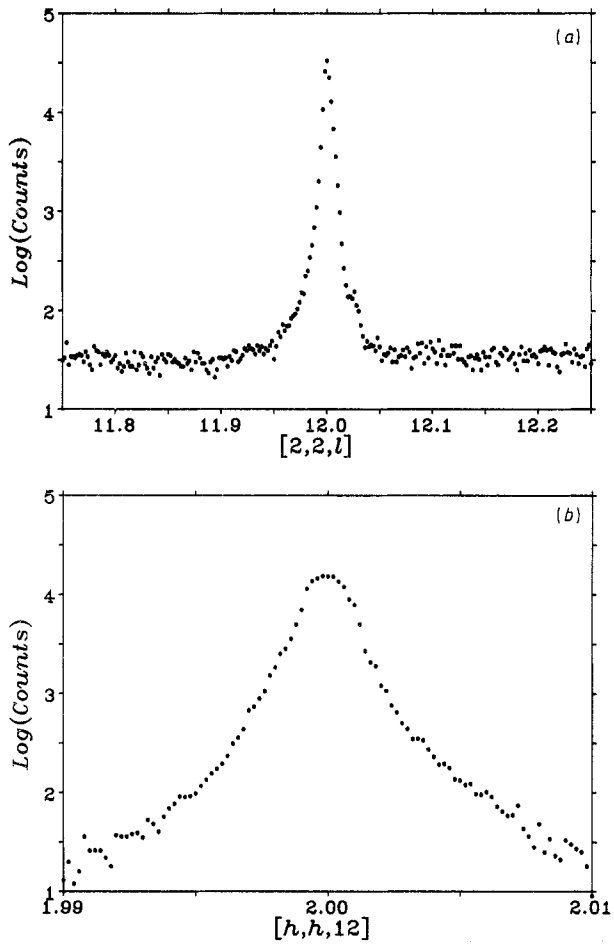

Figure 8. The x-ray scattering profiles of the (1, 1, 10) Bragg reflection measured in the paraelectric phase at 298 K for scans performed parallel (*a*) and perpendicular (*b*) to c^*. The high-resolution configuration was used for these measurements. Note: we have plotted the lower figure with an expanded Q scale.

$$f(\boldsymbol{Q}) = f_1(\boldsymbol{Q})(1 + \exp \mathrm{i}\boldsymbol{R}_B \cdot \boldsymbol{Q}) + \mathrm{i}f_2(\boldsymbol{Q})(1 - \exp \mathrm{i}\boldsymbol{R}_B \cdot \boldsymbol{Q})$$

where $\boldsymbol{R}_B = (\frac{1}{4}, \frac{1}{4}, 0)a$. If $\boldsymbol{Q}$ is a reciprocal lattice vector, (h, h, l), then when h is even

$$f(\boldsymbol{Q}) = 2f_1(\boldsymbol{Q})$$

while if h is odd

$$f(\boldsymbol{Q} = 2\,\mathrm{i}f_2(\boldsymbol{Q}).$$

The scattering along the lines $[h, h, l]$ with h even is then determined by $f_1(\boldsymbol{Q})$ which is the same for the A and B units, whereas the scattering with h odd depends on $f_2(\boldsymbol{Q})$ which represents the difference between the A and B units.

An understanding of the observed scattering profiles described in the last section can then be found from the above analysis. The units are arranged in regular sheets as shown in figure 1(*b*); along the ⟨110⟩ direction the sequence of the units is $ABABAB$, and the

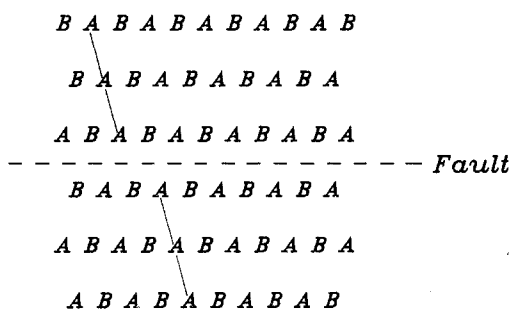

Figure 9. Schematic diagram showing a stacking fault in $TlGaSe_2$.

sheets above and below are displaced along ⟨110⟩ by $(\frac{1}{8}a, \frac{1}{8}b, 0)$. This ordered pattern gives rise to well-defined Bragg reflections. However, faults in the stacking of the sheets may occur as shown in figure 9, because the energy difference of the two positions for the sheets differs very little (the anisotropic nature of the bonding in $TlGaSe_2$ is indicated by the very low frequency of the rigid layer mode ($\simeq 15\ cm^{-1}$) observed by Volkov *et al* (1988)). The diffuse scattering along the lines with h odd then gives a measure of the number of the stacking faults of the planes.

In order to model the scattering from such a layered system with stacking faults, we have assumed that the probability of a plane having the incorrect position, figure 9, is p and of being correctly stacked is $1 - p$. The stacking can then be described for each sheet, n, by a spin variable $S(n)$ which is $+1$ if it is aligned correctly, as in figure 1(b), and -1 otherwise. The correlation function $\langle S(0)\, S(n)\rangle$, is identical to that of the one-dimensional Ising model, namely $(1 - 2p)^n$. The scattering cross-section is then given by the Fourier transform of the correlation function,

$$S(\boldsymbol{Q}) = \sum_n \exp(\mathrm{i}\, n\, \boldsymbol{Q}_c \cdot \boldsymbol{R}_c)\langle S(0)\, S(n)\rangle = \frac{2p(1-p)}{1 - 2p + 2p^2 - (1-2p)\cos(\boldsymbol{Q}_c \cdot \boldsymbol{R}_c)}$$

where $\boldsymbol{R}_c$ is the distance between the planes as shown in figure 1(a).

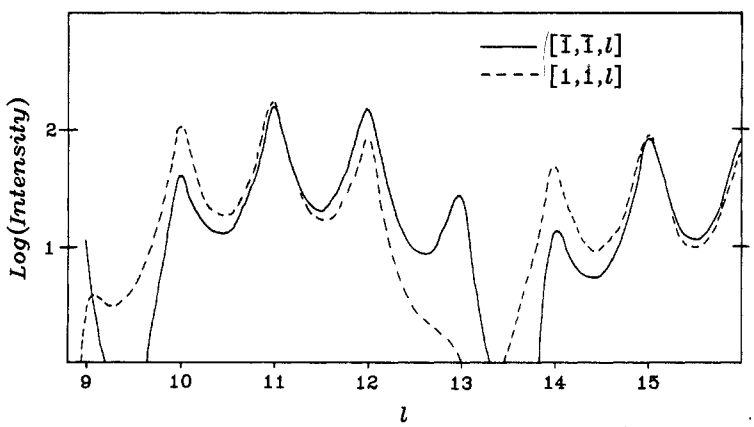

Figure 10. The scattering intensity calculated using the simple model described in section 3.2 for the lines $[\bar{1}, \bar{1}, l]$ and $[1, 1, l]$. The corresponding intensity for the $[\bar{3}, \bar{3}, l]$ line is identical to that for the $[1, 1, l]$ line except that l is reduced by one. Likewise, the intensity for the $[3, 3, l]$ line is the same as the $[\bar{1}, \bar{1}, l]$ line except l is increased by one.

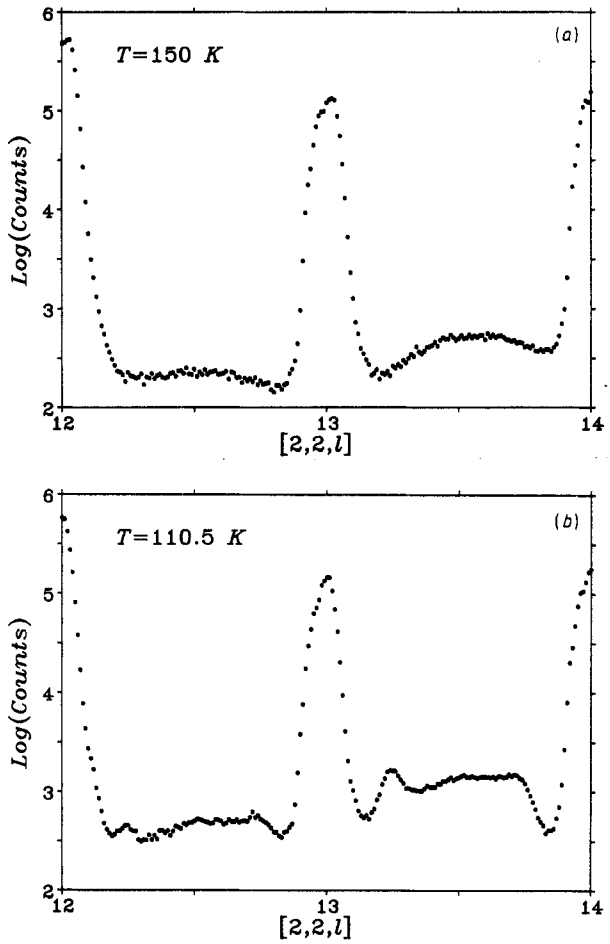

Figure 11. The x-ray intensity measured along the line [2, 2, *l*] in the paraelectric phase at 150 K (*a*) and at 110.5 K in the incommensurate phase (*b*). The low-resolution configuration was used for these measurements.

The intensity of the lines with $\boldsymbol{Q} = (h, h, l)$ and h odd is given by

$$I(\boldsymbol{Q}) = |f_2(\boldsymbol{Q})|^2 \, S(\boldsymbol{Q}).$$

This expression has been computed using the atomic positions perpendicular to ⟨110⟩ (Henkel *et al* 1982). We have neglected in our calculations the Debye–Waller factors and the $\boldsymbol{Q}$ dependence of the atomic form factors, while p was taken from the measured widths to be 0.25. The results of the calculations for the $[1, 1, l]$ and $[\bar{1}, \bar{1}, l]$ lines are shown in figure 10, and the general agreement with the experimental results is satisfactory. The minima in the calculated intensity shown in figure 10 arise from the zeros in $|f_2(\boldsymbol{Q})|^2$ and occur for $l = 9.4$ and 13.5 along the $[\bar{1}, \bar{1}, l]$ line. In the experiment the corresponding minima were found at 9.3 and 13.7; see figure 4. In view of the simplicity of the model the agreement between the observed and calculated positions of the minima is clearly satisfactory. Furthermore the shift in the minima from line to line

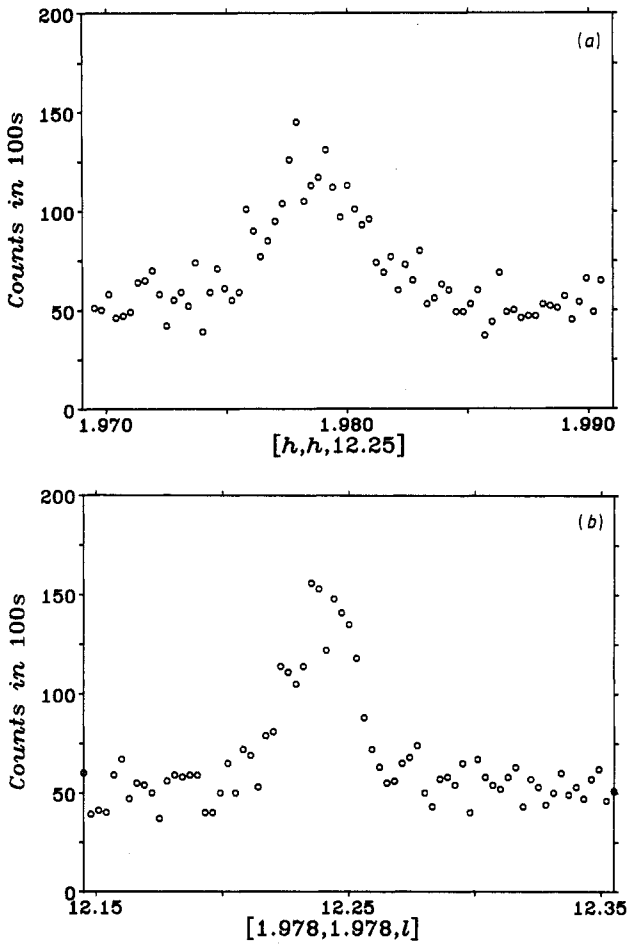

Figure 12. The x-ray scattering observed near the point (1.978, 1.978, 12.25) in the incommensurate phase at 111.3 K. The scans were performed in directions perpendicular (*a*) and parallel (*b*) to c^* using the high-resolution configuration.

is reproduced by our model. The calculated minima are much deeper than those observed because we did not include scattering by other processes or the background in our model.

In detail the scattering near the Bragg reflections has a more complex structure than that given by our simple model. This is presumably because the probability of a stacking fault is not described by a simple probability, but rather there exist more complex correlations between the defects. Nevertheless the success of such a simple model does show that in the crystal used, there was imperfect stacking, with a fault occurring approximately once in every four planes.

The possible occurrence of disorder in the stacking sequence along c^* in $TlGaSe_2$ was first mooted by Müller and Hahn (1978) in their structural study. Moreover, the existence of polytynic structures in $TlGaSe_2$, similar to those that are known to occur in materials such as CdI_2, SiC etc (Michalski 1988 and references therein), was predicted by Abdullaeva *et al* (1980).

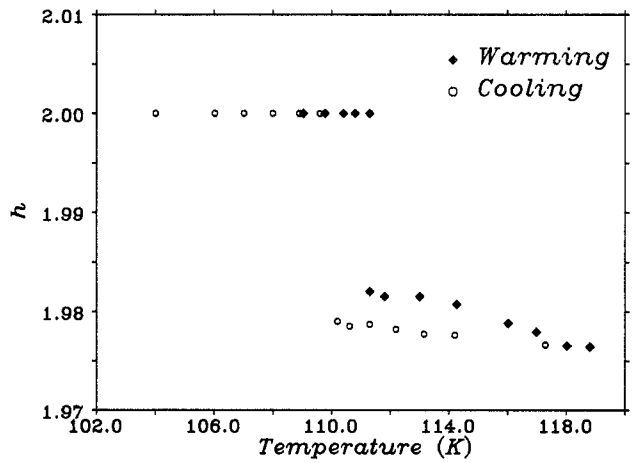

Figure 13. The temperature dependence of the position of the incommensurate satellite near the position (1.978, 1.978, 12.25) along the [h, h, 12.25] direction. The open circles and filled diamonds represent respectively the data collected in cooling and warming cycles.

4. The incommensurate phase

Experiments were performed to search for the proposed incommensurate phase in $TlGaSe_2$ by cooling the sample towards 100 K. The results obtained with the low resolution configuration are shown in figure 11. There is a steady increase in the scattering at points in reciprocal space corresonding to a quadrupoling of the unit cell along c^* as found in $TlInS_2$ (Vakhrushev *et al* 1984b). No incommensurate peaks were, however, found with this configuration. The high-resolution configuration, with germanium crystals as monochromator and analyser, enabled satellite peaks to be observed below 120 K as shown in figure 12. The peaks correspond to a modulation wavevector $\boldsymbol{q}_i = (\delta, \delta, \frac{1}{4})$ with $\delta \simeq 0.02$. From figure 12 it is clear that the incommensurate peak is very weak (1 count s^{-1} above background), and that its width along the c^* axis is approximately seven times larger than the width along [110] both being considerably larger than the experimental resolution. Unfortunately, as the scattering from the incommensurate modulation was very weak, it was not possible to collect accurate integrated intensities, and we cannot therefore comment on the structural distortion giving rise to the incommensurate peaks.

When the temperature was lowered further, δ was observed to decrease somewhat, and then, at about 110 K, jumped discontinuously to zero. The results of detailed measurements of the variation of δ with temperature are given in figure 13. On warming from below 110 K, the structure remains commensurate to $\simeq$111.3 K. This hysteresis in the transition temperature and the magnitude of the modulation wavevector is characteristic of many incommensurate–commensurate transitions.

5. The low-temperature structure

The scattering at low temperatures is illustrated in figure 14. Relative to the high-temperature phase there are additional peaks with $\boldsymbol{q}_c = (0, 0, \frac{1}{4})$ around many of the Bragg reflections, for both h odd and h even. This agrees with the neutron diffraction study of Vakhrushev *et al* (1984a). The satellite reflections with $\boldsymbol{q}_c = (0, 0, \frac{1}{4})$ were more

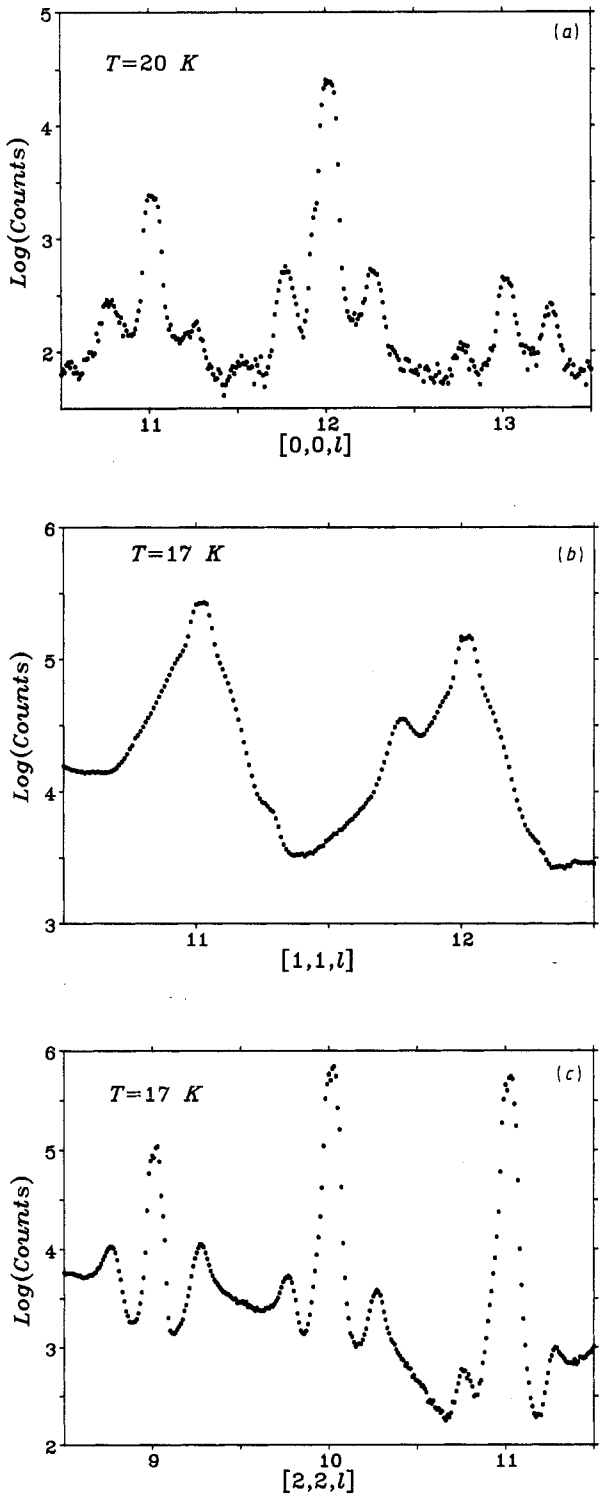

Figure 14. The results of scans taken at low temperatures using the low-resolution configuration showing weak scattering at $[h, h, l + \frac{1}{4}]$ for $h = 0$ (a), $h = 1$ (b) and $h = 2$ (c).

difficult to observe for odd values of h because of the diffuse scattering discussed in section 3. There is little evidence for peaks with $\boldsymbol{q} = (0, 0, \frac{1}{2})$, and indeed the additional low-temperature peaks are always weak showing that the structure is only slightly distorted. We have not attempted a full structural analysis of this phase, but it is worth commenting that our results show that there are motions along $\boldsymbol{c}^*$ perpendicular to the axis along which the dielectric constant is a maximum at 110 K (Aliev *et al* 1984).

6. Conclusions

In this paper we have presented the results of detailed x-ray scattering measurements from $TlGaSe_2$ in its paraelectric and incommensurate phases, in addition to less detailed measurements of its low-temperature, ferroelectric phase. In the paraelectric phase above $T_i = 117$ K, we found that the (*hhl*) Bragg reflections with h odd had diffuse tails extending along $\boldsymbol{c}^*$, whereas reflections with h even were resolution limited. An adequate description of the scattering along [*hhl*] with h odd was obtained by assuming that faults in the stacking of the atomic planes perpendicular to $\boldsymbol{c}^*$ occurred every fourth layer. The first direct evidence for the existence of an incommensurate phase below 117 K in this compound was reported. The modulation wavevector of the incommensurate phase found to be $\boldsymbol{q}_i = (\delta, \delta, \frac{1}{4})$, where δ decreases discontinuously to zero at 110 K. The scattering from the low-temperature, ferroelectric phase indicated a quadrupling of the c lattice parameter.

Acknowledgments

Financial support for this work was provided by the Science and Engineering Research Council. Hugh Vass provided excellent technical support for the experiments.

References

Abdullaev G B, Allakhverdiev K R, Vinogradov E A, Zhizhin G N, Nani R Kh, Salaev E Yu and Sardarly R M 1977 *Dokl. Akad. Nauk* **33** 26

Abdullaeva S G, Abdinbekov S S and Guseinov G G 1980 *Dokl. Akad. Nauk* **36** 34

Aliev R A, Allakhverdiev K R, Baranov A I, Ivanov N R and Sardarly R M 1984 *Sov. Phys.–Solid State* **26** 775

Banys Yu, Brilingas A, Grigas I and Guseynov G D 1987 *Sov. Phys.–Solid State* **29** 1906

Cowley R A 1987 *Acta. Crystallogr.* A **43** 825

Durnev Yu I, Kulbuzhev B S, Malsagov A U, Rabkin L M, Torgashev V I and Yuzyk Yu I 1989 *Phys. Status Solidi* b **153** 517

Guseinov G D, Ramazanzade A N, Kerimova E M and Ismailov M Z 1967 *Phys. Status Solidi* b **22** K117

Henkel W, Hochheimer H D, Carlone C, Werner A, Ves S and von Schnering H G 1982 *Phys. Rev.* B **26** 3211

Lucas C A, Gartstein E and Cowley R A 1989 *Acta Crystallogr.* A **45** 416

Michalski E 1988 *Acta Crystallogr.* A **44** 640

Müller D and Hahn H 1978 *Z. Anorg. (Allg.) Chem.* **438** 258

Offergeld G R 1963 *US Patent 3* **110** 685

Vakhrushev S B, Kryatkovsky B E, Okuneva N M, Allakhverdiev K M and Sardarly R M 1984a *Preprint* 886 Physico-Technical Institute, Leningrad

Vakhrushev S B, Zhdanova V V, Kryatkovsii B E, Okunenva N M, Allakhverdiev K R, Aliev R A and Sardarly R M 1984b *JETP Lett.* **39** 291

Volkov A A, Goncharov Yu G, Kozlov G V, Lebedev S P, Prokhorov A M, Aliev R A and Allakhverdiev K R 1983 *JETP Lett.* **37** 615